Hysteresis in the metachronal-tripod gait transition of insects: A modeling study

AUTHOR(S):

Fujiki, Soichiro; Aoi, Shinya; Funato, Tetsuro; Tomita, Nozomi; Senda, Kei; Tsuchiya, Kazuo

CITATION:

Fujiki, Soichiro ...[et al]. Hysteresis in the metachronal-tripod gait transition of insects: A modeling study. Physical Review E 2013, 88(1): 012717.

ISSUE DATE:

2013-07-15

URL:

http://hdl.handle.net/2433/188008

PHYSICAL REVIEW E **88**, 012717 (2013)

Hysteresis in the metachronal-tripod gait transition of insects: A modeling study

Soichiro Fujiki,[1] Shinya Aoi,[1,4] Tetsuro Funato,[2,4] Nozomi Tomita,[3,4] Kei Senda,[1] and Kazuo Tsuchiya[3,4]

[1]*Department of Aeronautics and Astronautics, Graduate School of Engineering, Kyoto University, Kyoto daigaku-Katsura, Nishikyo-ku, Kyoto 615-8540, Japan*

[2]*Department of Mechanical Engineering and Intelligent Systems, Graduate School of Informatics and Engineering, The University of Electro-Communications, 1-5-1 Chofugaoka, Chofu, Tokyo 182-8585, Japan*

[3]*Department of Energy and Mechanical Engineering, Faculty of Science and Engineering, Doshisha University, 1-3 Tatara, Miyakodani, Kyotanabe, Kyoto 610-0394, Japan*

[4]*JST, CREST, 5 Sanbancho, Chiyoda-ku, Tokyo 102-0075, Japan*

(Received 18 March 2013; published 15 July 2013)

Locomotion in biological systems involves various gaits, and hysteresis appears when the gaits change in accordance with the locomotion speed. That is, the gaits vary at different locomotion speeds depending on the direction of speed change. Although hysteresis is a typical characteristic of nonlinear dynamic systems, the underlying mechanism for the hysteresis in gait transitions remains largely unclear. In this study, we construct a neuromechanical model of an insect and investigate the dynamic characteristics of its gait and gait transition. The simulation results show that our insect model produces metachronal and tripod gaits depending on the locomotion speed through dynamic interactions among the body mechanical system, the nervous system, and the environment in a self-organized manner. They also show that it undergoes the metachronal-tripod gait transition with hysteresis by changing the locomotion speed. We examined the hysteresis mechanism in the metachronal-tripod gait transition of insects from a dynamic viewpoint.

DOI: 10.1103/PhysRevE.88.012717 PACS number(s): 87.19.ru, 87.85.gj, 87.19.lj

I. INTRODUCTION

Biological systems have various gaits in their locomotion and the gaits are characterized by the number of legs used for locomotion. Humans walk bipedally and use walking and running gaits in accordance with the locomotion speed. Quadrupeds have four legs and employ various gaits such as walking, trotting, and galloping. Insects (hexapods) with six legs use metachronal (wave) and tripod gaits. These gaits are characteristic locomotion patterns that are generated over a limited range of locomotion speeds, and they are described by parameters that vary discontinuously at the transition [1]. In the walk-run transition of humans, the relative phase between the leg segments [that is, the intralimb (or intersegmental) coordination pattern] varies [2]. In contrast, in the walk-trot-gallop transition of quadrupeds and the metachronal-tripod gait transition of insects, the relative phase between the legs (i.e., the interlimb coordination pattern) changes [1,3].

Locomotion is a self-organizing phenomenon that emerges through dynamic interactions among the nervous system, the musculoskeletal system, and the environment and it has a number of nonlinear characteristics. In particular, hysteresis appears when the gaits change in accordance with the locomotion speed [2,4–11]. Specifically, the gaits vary at different locomotion speeds depending on the direction of speed change. Although hysteresis is a typical characteristic of nonlinear dynamic systems, the hysteresis mechanism in the gait transition of biological systems remains largely unclear.

So far, to elucidate the locomotor mechanisms in biological systems, biomechanical and physiological studies have been independently conducted. Biomechanical studies generally focus on the functional roles of the musculoskeletal system, whereas physiological studies mainly examine the configurations and activities of the neural system. However, locomotion is a well-organized motion generated through the body and the nervous system and it is thus difficult to fully elucidate the locomotor mechanisms from a single perspective. To overcome the limitations of studies based on a single approach, neuromechanical models for the locomotion of biological systems have been developed by integrating the biomechanical and physiological findings [12–23].

From the observation of locomotion, hysteresis has been reported in the walk-run transition of humans [2,6–9,11] and in the gait transitions of quadrupeds [4,5,10]. Neuromechanical models of humans and quadrupeds have been employed to investigate their gait transition mechanisms and have demonstrated that hysteresis appears in the walk-run transition of humans [21] and in the walk-trot transition of quadrupeds [12]. However, regarding insect locomotion, although the gaits of insects have been investigated [3,24–28], to the best of our knowledge it remains unclear if hysteresis appears in the gait transitions of insects.

To date, oscillator network models have been used to examine the gait transition in insect locomotion [26,29–31]. However, these models did not incorporate the contribution of the body mechanical system. In contrast, neuromechanical models for insect locomotion have been developed and help the understanding of the contributions of sensory-motor coordination to the generation of locomotion [13–16,20,22,23], but they did not investigate the gait transition mechanism. The aim of this study is to construct a neuromechanical model of an insect and to investigate the dynamic characteristics of its gait and gait transition. Specifically, we investigate what gaits our model produces depending on the locomotion speed and if the gaits vary when the locomotion speed is changed. Furthermore, we examine whether the gait transitions exhibit hysteresis and what dynamic structures produce the gait transitions.

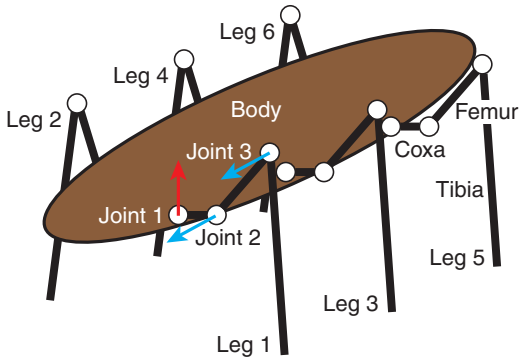

FIG. 1. (Color online) Body mechanical model of an insect consisting of a body and six legs.

II. METHODS

A. Body mechanical model

Figure 1 shows the body mechanical model of an insect, which consists of one rigid body and three pairs of legs (legs 1–6). Each leg has three rigid links (coxa, femur, and tibia). The body-coxa, coxa-femur, and femur-tibia joints are enumerated as joints 1, 2, and 3, respectively. Joint 1 moves the leg tip forward or backward relative to the body, and joints 2 and 3 raise or lower the leg tip. Leg joint movements are generated by motor commands from the nervous system model (see Sec. II B).

We derived the equation of motion of this body mechanical model using a Lagrangian equation as in [12], where we used viscoelastic elements to model the contact between the leg tips and the ground and used large values for the viscoelastic parameters so that the leg tips rarely slipped during foot contact. We performed forward dynamic simulations by solving the equation of motion using a fourth-order Runge-Kutta method with a step size of 0.02 ms. Table I shows the physical parameters of the insect model; the six legs had the same parameter values as each other.

B. Nervous system model

Physiological studies have shown that central pattern generators (CPGs) greatly contribute to producing motor commands for rhythmic leg movements in both vertebrates and invertebrates [32–36], which are located in the spinal cord of vertebrates and in the thoracic ganglia of invertebrates. Although the organization of CPGs remains unclear, physiological findings suggest that CPGs consist of hierarchical networks composed of rhythm generator (RG) and pattern formation (PF) networks [37–39]. The RG network produces the basic rhythm and the PF network shapes the rhythm into spatiotemporal patterns of motor commands. In this study, we modified the oscillator network model, which is a simple two-layer network system composed of RG and PF models and which is constructed for quadruped locomotion [12], to apply it for the nervous system model of an insect (Fig. 2).

TABLE I. Physical parameters of the insect model.

Link	Parameter	Value
Body	Mass (g)	3.0
	Length (cm)	4.2
	Width (cm)	1.0
Coxa	Mass (g)	0.05
	Length (cm)	0.02
Femur	Mass (g)	0.03
	Length (cm)	0.2
Tibia	Mass (g)	0.03
	Length (cm)	1.0

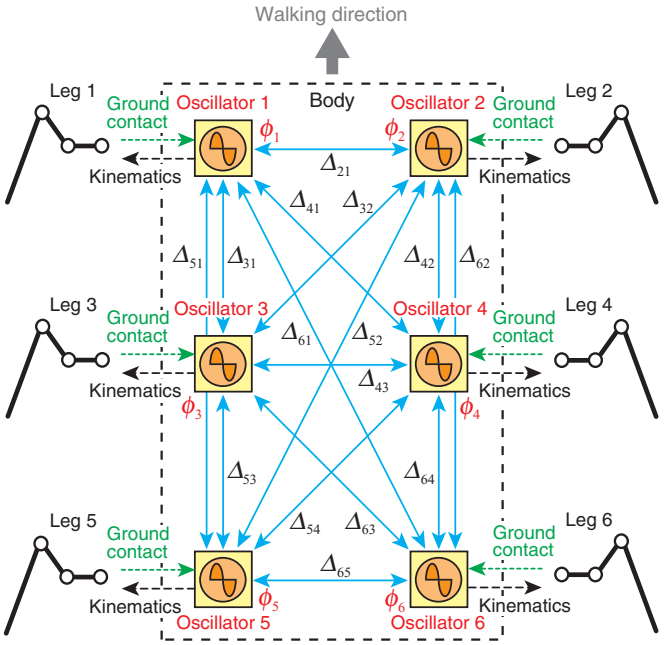

FIG. 2. (Color online) Nervous system model using six oscillators. Solid blue arrows indicate interactions among the oscillators based on the phase relationship Δ_{ij}. The oscillator phases are modulated by tactile sensor information (dotted green arrows). The oscillator phases determine the leg joint kinematics (dashed black arrows).

1. Rhythm generator model

The RG model produces rhythm information for locomotion through dynamic interactions among the body mechanical system, the nervous system, and the environment. For the RG model, we used six simple phase oscillators (oscillators 1–6) to generate the basic rhythm and phase information for the corresponding leg based on commands related to the desired locomotion speed and gait. We denote the phase of the oscillator i ($i = 1, \ldots, 6$) by ϕ_i ($0 \leqslant \phi_i < 2\pi$) and used the following phase dynamics:

$$\dot{\phi}_i = \omega + g_{1i} + g_{2i}, \quad i = 1, \ldots, 6, \tag{1}$$

where ω is the basic oscillator frequency (it has the same value for all six oscillators), g_{1i} is the interaction between the oscillators based on the interlimb coordination (see Sec. II B3), and g_{2i} is the sensory regulation based on a phase resetting mechanism (see Sec. II B4).

2. Pattern formation model

Physiological studies have revealed that nervous systems receive sensory information and encode global parameters of

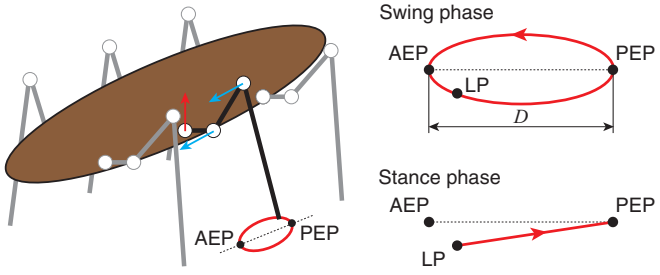

FIG. 3. (Color online) Leg joint kinematics composed of swing and stance phases. The swing phase for the leg tip is a closed curve that includes the anterior extreme position (AEP) and the posterior extreme position (PEP). The stance phase is a straight line from the landing position (LP) to the PEP. When the leg lands on the ground, it changes from the swing to the stance phase. When the leg tip reaches the PEP, it moves into the swing phase.

the leg kinematics, such as the length and orientation of the limb axis (position of the leg tip relative to the root) [40–43]. We used the PF model to determine the leg kinematics based on the oscillator phase ϕ_i from the RG model and to produce motor torques for generating the desired kinematics.

Locomotion involves propelling the center of mass forward, which is achieved by moving the swing leg forward and by supporting the body and producing a propulsive force from the ground using the stance leg. We used a simple leg kinematics composed of the swing and stance phases (Fig. 3). The swing phase consists of a simple closed curve for the leg tip that includes the anterior extreme position (AEP) and the posterior extreme position (PEP). It starts from the PEP and continues until the leg touches the ground. The line segment between the AEP and the PEP is parallel to the body. The stance phase is a straight line from the landing position (LP) to the PEP. During this phase, the leg tip moves in the opposite walking direction relative to the body. The body travels in the walking direction while the leg tips are in contact with the ground.

We used D for the distance between the AEP and the PEP. We denote the swing and stance phase durations by $T_{\rm sw}$ and $T_{\rm st}$, respectively, for the case when the leg tip contacts the ground at the AEP (LP = AEP). The duty factor β (the ratio between the stance phase and the step cycle duration), the basic frequency ω in (1), the locomotion speed v, and the stride length S are, respectively, given by

$$\beta = \frac{T_{\rm st}}{T_{\rm sw}+T_{\rm st}}, \quad \omega = \frac{2\pi}{T_{\rm sw}+T_{\rm st}} = \frac{2\pi(1-\beta)}{T_{\rm sw}}, \\ v = \frac{D}{T_{\rm st}} = \frac{(1-\beta)D}{\beta T_{\rm sw}}, \quad S = D + vT_{\rm sw} = \frac{D}{\beta}. \tag{2}$$

We used $D = 2$ mm and $T_{\rm sw} = 34$ ms and varied v by changing β through $T_{\rm st}$ in the same manner as observed in the locomotion of biological systems [25,28,35,44,45], where ω and S also vary with β. We used the same values of these parameters for all the legs.

These trajectories for the swing and stance phases are given as functions of the corresponding oscillator phase, where we used $\phi_i = 0$ at the PEP and $\phi_i = \phi_{\rm AEP}[= 2\pi(1-\beta)]$ at the AEP. Therefore, the desired joint kinematics is given as a function of the oscillator phase and each joint is controlled by the joint torque based on proportional-derivative (PD) feedback control to produce the desired kinematics.

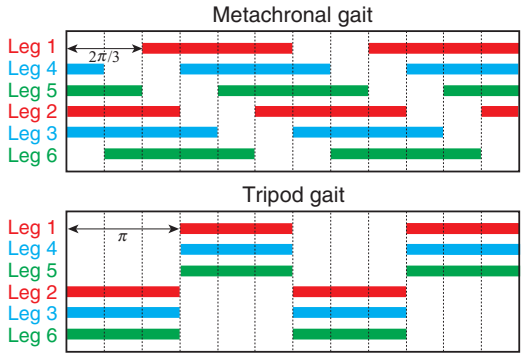

FIG. 4. (Color online) Footprint diagrams for metachronal and tripod gaits, where the right and left legs move in antiphase [red, fore legs (legs 1 and 2); blue, middle legs (legs 3 and 4); green, hind legs (legs 5 and 6)].

3. Gait pattern

Because the leg kinematics is determined by the corresponding oscillator phase, the interlimb coordination pattern is determined by the relative phase between the oscillators. We denote the relative phase by the matrix $\Delta_{ij} = \phi_i - \phi_j$ $(i,j = 1,\ldots,6,\ 0 \leqslant \Delta_{ij} < 2\pi)$. As the relationships $\Delta_{ij} = -\Delta_{ji}$, $\Delta_{ij} = \Delta_{ik} + \Delta_{kj}$, and $\Delta_{ii} = 0$ $(i,j,k = 1,\ldots,6)$ are satisfied, the gait is determined by five state variables, such as $[\Delta_{21}\ \Delta_{31}\ \Delta_{43}\ \Delta_{53}\ \Delta_{65}]$. For example, $[\Delta_{21}\ \Delta_{31}\ \Delta_{43}\ \Delta_{53}\ \Delta_{65}] = [\pi\ 2\pi/3\ \pi\ 2\pi/3\ \pi]$ is satisfied for the metachronal gait and $[\Delta_{21}\ \Delta_{31}\ \Delta_{43}\ \Delta_{53}\ \Delta_{65}] = [\pi\ \pi\ \pi\ \pi\ \pi]$ is satisfied for the tripod gait (Fig. 4).

Function g_{1i} in (1) manipulates these relative phases, which is given by

$$g_{1i} = -\sum_{j=1}^{6} K_{ij}\sin(\Delta_{ij} - \Delta^*_{ij}), \quad i = 1,\ldots,6, \tag{3}$$

where Δ^*_{ij} $(i,j = 1,\ldots,6)$ is the desired relative phase and K_{ij} $(i,j = 1,\ldots,6)$ is the gain constant $(K_{ij} \geqslant 0)$. When a large value is used for K_{ij}, the relationship $\Delta_{ij} = \Delta^*_{ij}$ is satisfied. The solid blue arrows in Fig. 2 indicate these interactions among the oscillators.

4. Phase resetting

To produce adaptive and effective locomotor behaviors, adequate sensory regulation of motor commands is crucial. Physiological studies have shown that the locomotor rhythm and phase are modulated by producing phase shift and rhythm resetting based on sensory afferents and perturbations (phase resetting) [32,39,46–48]. In addition, neuromusculoskeletal models have demonstrated the contributions of phase resetting to the generation of adaptive locomotion [49–52].

In this study, we incorporated the phase resetting mechanism to produce adaptive locomotion through dynamic interactions among the body mechanical system, the nervous system, and the environment. Because cutaneous afferents were observed to contribute to these resetting behaviors [47,48], we reset the phase ϕ_i of the oscillator i to $\phi_{\rm AEP}$ when

the leg i lands on the ground ($i = 1, \ldots, 6$). Function g_{2i} in (1) corresponds to this resetting and is given by

$$g_{2i} = (\phi_{\mathrm{AEP}} - \phi_i)\delta\left(t - t^i_{\mathrm{land}}\right), \quad i = 1, \ldots, 6, \tag{4}$$

where t^i_{land} is the time when the leg i contacts the ground ($i = 1, \ldots, 6$) and $\delta(\cdot)$ denotes the Dirac delta function. The tactile sensor signals not only modulate the locomotion rhythm and phase but also switch the leg movements from the swing to the stance phase, as described in Sec. II B2.

5. *Constraints for gait*

The relative phase between the oscillators determines the gait of our model, which is produced by the interactions among the oscillators (3) and the sensory regulation by phase resetting (4). When we use neither (3) nor (4), the relative phase remains in the initial state and the gait does not change. When all the elements of matrix Δ^*_{ij} are determined based on the desired gait and large values are used for the gain constants K_{ij} in (3), our model will establish the desired gait when the gait becomes stable. In contrast, when small values are used for K_{ij}, this can generate a different gait from the desired one due to the sensory regulation by phase resetting (4).

Based on the relationship of the leg movements in the locomotion of insects [3], we employed some constraints for the relative phase Δ_{ij}. Because the right and left legs move in antiphase, we used

$$\Delta^*_{21} = \Delta^*_{43} = \Delta^*_{65} = \pi, \tag{5}$$

and a large value for K_{12}, K_{21}, K_{34}, K_{43}, K_{56}, and K_{65} ($K_{12} = K_{21} = K_{34} = K_{43} = K_{56} = K_{65} = 32$). In addition, because the intervals between the steps of the fore leg and middle leg and between the middle leg and hind leg are identical (they vary with the locomotion speed), we consider

$$\Delta_{31} = \Delta_{53}\ (\Delta_{42} = \Delta_{64}). \tag{6}$$

To satisfy this condition, we modified the following desired phases using the actual relative phases by

$$\Delta^*_{31} = \Delta_{53}, \quad \Delta^*_{35} = \Delta_{13}, \quad \Delta^*_{42} = \Delta_{64}, \quad \Delta^*_{46} = \Delta_{24}, \tag{7}$$

and used a large value for K_{31}, K_{35}, K_{42}, and K_{46} ($K_{31} = K_{35} = K_{42} = K_{46} = 40$).

From the conditions (5) and (6), $\Delta_{21} = \Delta_{43} = \Delta_{65} = \pi$ and $\Delta_{31} = \Delta_{53}$ are generally satisfied so that there are four constraints for the five state variables of the gait. Because we set the other K_{ij} to zero, the gait is determined by a single phase relationship, such as Δ_{31}, which is obtained through the locomotion dynamics. For example, our model establishes a metachronal gait when $\Delta_{31} = 2\pi/3$ and a tripod gait when $\Delta_{31} = \pi$ (Fig. 4).

III. RESULTS

A. Dependence of metachronal and tripod gaits on locomotion speed

We first investigated the gaits that our model generates at $\beta = 0.62$ ($v = 3.6$ cm/s) and 0.7 ($v = 2.5$ cm/s). Specifically, we used three initial values for the relative phase Δ_{31} and examined where Δ_{31} converged.

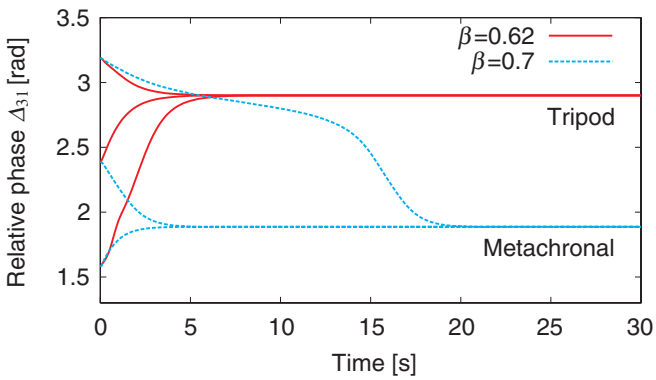

FIG. 5. (Color online) Relative phase Δ_{31} plotted at contact of leg 1 for three initial values with $\beta = 0.62$ and 0.7. For $\beta = 0.62$ Δ_{31} converges to 2.9 rad (tripod), while Δ_{31} converges to 1.9 rad (metachronal) for $\beta = 0.7$.

Figure 5 shows the results of Δ_{31}, plotted when leg 1 touches the ground. For $\beta = 0.62$, Δ_{31} converged to 2.9 rad, indicating that our model established the tripod gait at high speed. In contrast, Δ_{31} converged to 1.9 rad for $\beta = 0.7$, indicating that our model performed the metachronal gait at low speed. Our model produced different gaits depending on the locomotion speed.

B. Appearance of hysteresis in gait transition

After our model produced a stable gait, we slowly increased the locomotion speed by reducing the duty factor β from 0.7 to 0.62 or we reduced the locomotion speed by increasing β from 0.62 to 0.7. We investigated how the gait changed through locomotion dynamics.

Figure 6(a) shows the results of Δ_{31} for increasing and decreasing the locomotion speed. It varied between 2.9 and 1.9 rad, indicating that the gait changed between the metachronal and tripod gaits. When we reduced the locomotion speed, the tripod gait transitioned to the metachronal gait at about $\beta = 0.67$. In contrast, when we increased the locomotion speed, the metachronal gait changed to the tripod gait at about $\beta = 0.645$. This means that the gait transition occurs at different locomotion speeds depending on the direction of the speed change, i.e., hysteresis appears. Figure 6(b) shows the footprint diagram during the metachronal-to-tripod gait transition.

C. Stability characteristics in the hysteresis

Based on our previous work [12], we clarify the stability structure of locomotion dynamics that induces the hysteresis in the gait transition. In particular, we use the return map of Δ_{31} by plotting the relationship between Δ_{31n} at the foot contact of leg 1 for the nth gait cycle and Δ_{31n+4} for the $(n+4)$th gait cycle. We can determine possible gaits and their stabilities from the intersection with the diagonal line ($\Delta_{31n+4} = \Delta_{31n}$). Specifically, the intersection corresponds to the equilibrium point for the gait, and when the slope at the intersection is less than 1 and larger than -1, the equilibrium point is asymptotically stable. When the slope is larger than 1 or less than -1, the equilibrium point is unstable. The return

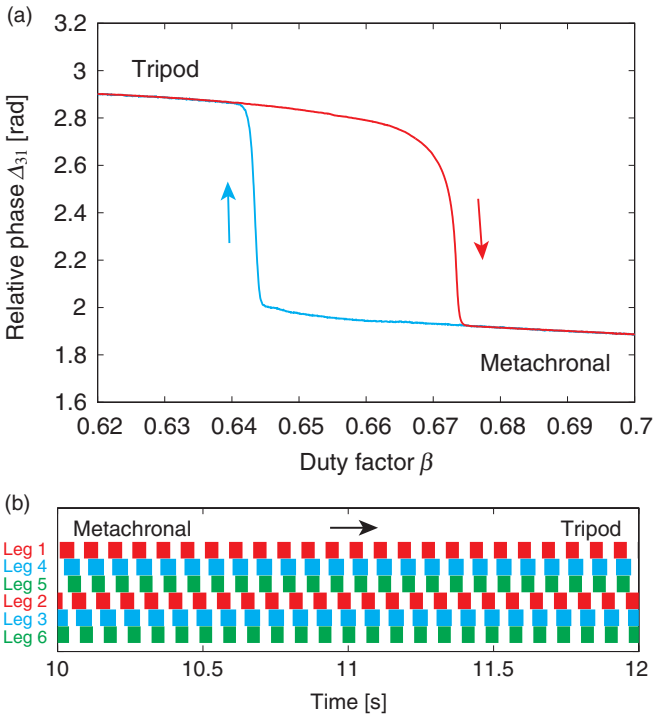

FIG. 6. (Color online) Gait transition induced by changing the locomotion speed through duty factor β. (a) Relative phase Δ_{31}. Metachronal-to-tripod and tripod-to-metachronal gait transitions occur at different locomotion speeds and hysteresis appears. (b) Footprint diagram during metachronal-to-tripod gait transition.

map elucidates not only the local stability, but also the global stability for the gait dynamics.

Figure 7 shows the results of the return map for $\beta = 0.64$, 0.655, and 0.675. For $\beta = 0.64$, there is only one intersection with a diagonal line, and the tripod gait is the only attractor. When $\beta = 0.655$, three intersections appear and there are two stable gaits (tripod and metachronal) and one unstable gait between the stable gaits (indicated by the open dot). For $\beta = 0.675$, the tripod gait disappears, which the loss of the two

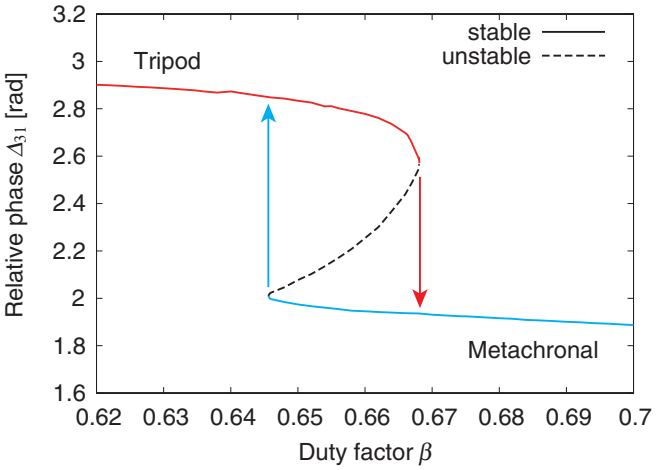

FIG. 8. (Color online) Stable and unstable gaits calculated from the return maps. Two stable gaits and one unstable gait coexist from $\beta = 0.645$ to 0.67. Fold catastrophe occurs at connections of the stable and unstable gaits and induces jump of gaits.

intersections reflects, and the metachronal gait becomes the only attractor. That is, the gait stability passes through the saddle-node bifurcation twice. A ghost [53] appears close to the saddle-node bifurcations, as shown around $\Delta_{31n} = 2.0$ rad for $\beta = 0.64$ and $\Delta_{31n} = 2.8$ rad for $\beta = 0.675$.

Figure 8 shows the stable and unstable gaits obtained by calculating the return map for each locomotion speed. The tripod gait is stable from $\beta = 0.62$ to 0.67, while the metachronal gait is stable from $\beta = 0.645$ to 0.7, indicating that two different stable gaits coexist from $\beta = 0.645$ to 0.67. These stable gaits are connected by the unstable gait, showing the fold catastrophe. These stability structures induce a jump of the gait as shown by the arrows, which give rise to the hysteresis.

D. Dependence of the gait transition on other physical conditions

In addition to the locomotion speed, we also investigated the effects of other physical conditions on the gait transition. In

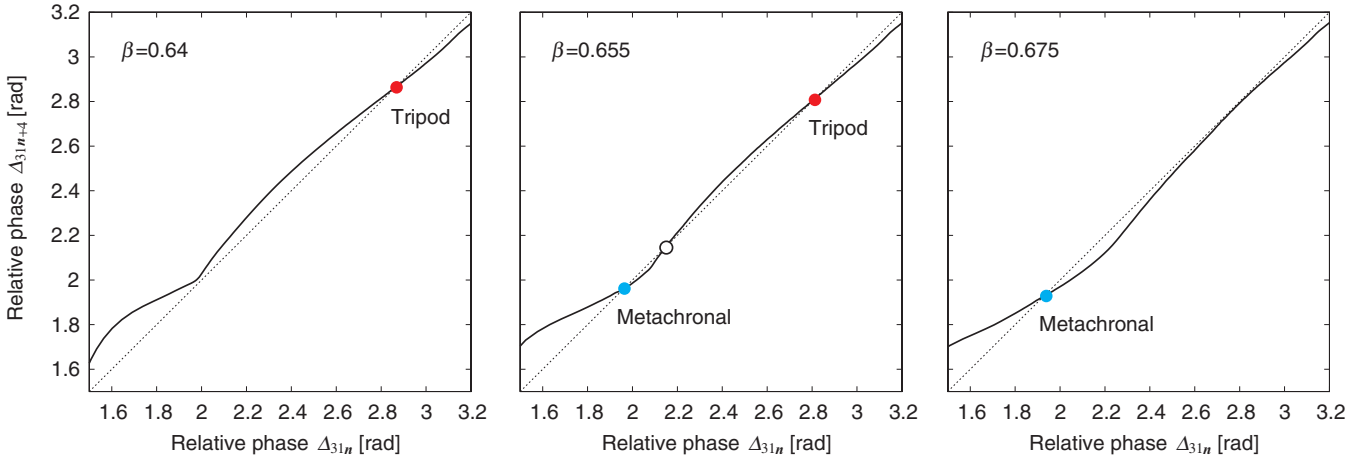

FIG. 7. (Color online) Return maps of the relative phase Δ_{31} for $\beta = 0.64$, 0.655, and 0.675 by plotting the relationship between the relative phase Δ_{31n} for the nth gait cycle and the relative phase Δ_{31n+4} for the $(n+4)$th gait cycle. Solid and open dots indicate stable and unstable gaits, respectively.

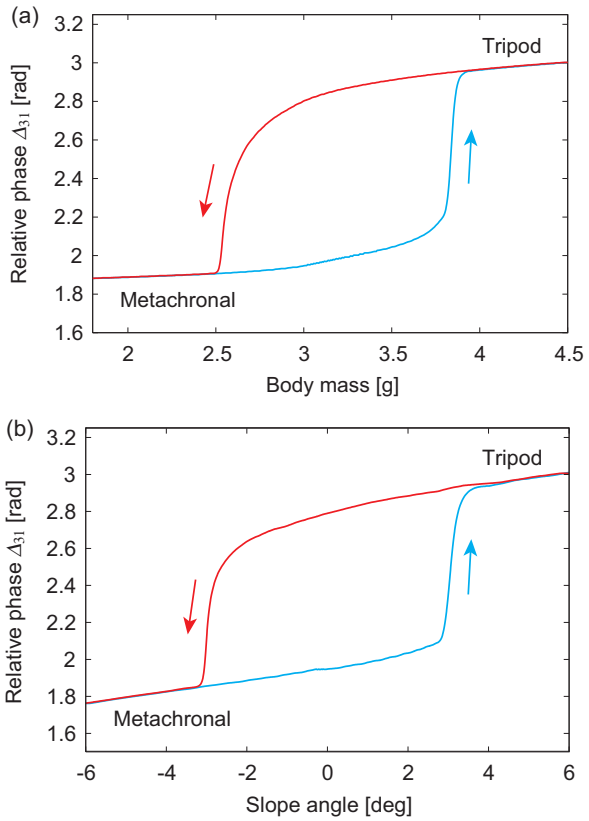

FIG. 9. (Color online) Gait transition induced by changing (a) body mass and (b) slope angle. Positive slope angle indicates uphill. Tripod gait is produced for large body mass and uphill walking, whereas metachronal gait is generated for small body mass and downhill walking. Hysteresis appears when body mass and slope angle are changed.

particular, we slowly changed the mass of the body or the slope angle of the ground, where we used $\beta = 0.66$, and examined what changes are induced on the gait.

Figure 9(a) shows the result of Δ_{31} when the body mass was changed. Our model established the tripod gait for a large body mass, whereas it produced the metachronal gait for a small body mass. In addition, hysteresis occurred when the body mass was changed, as observed when the locomotion speed was changed [Fig. 6(a)].

Figure 9(b) shows the result for the change in the slope angle, where a positive slope angle indicates uphill (we used a mass of 3.0 g for the body). Our model attained the tripod gait for uphill walking, whereas it achieved the metachronal gait for downhill walking. Hysteresis also appeared when the slope angle was changed.

Gait transitions of biological systems are affected by various physical conditions and environments. For example, when horses carry weights [54] or when they walk up an incline [55], the trot-to-gallop transition speed is reduced. Regarding the locomotion of cockroaches, while they use the tripod gait during normal walking, it changes to the metachronal gait when they are tethered on a supported ball to decrease loading [56]. Although the tripod gait remains during uphill walking, it changes to the metachronal gait during downhill walking. Loading and uphill walking induce similar effects on their gaits [57]. Our simulation results show that only the tripod gait is stable for increased loading and the metachronal gait is stable for decreased loading [Fig. 9(a)]. In addition, while the tripod gait is stable during uphill walking, it changes to the metachronal gait during downhill walking [Fig. 9(b)]. Our results are consistent with these observations.

IV. DISCUSSION

In this study, we developed a neuromechanical model of an insect to emulate its dynamic locomotion. Our model established the metachronal gait at slow locomotion speeds and the tripod gait at fast locomotion speeds, as observed in insect locomotion [3,25,28]. Furthermore, it exhibited a metachronal-tripod gait transition with hysteresis (Fig. 6). In addition to the locomotion speed, the changes in the mass of the body and the slope angle of the ground also produced the gait transition with hysteresis (Fig. 9). These results were not because we designed the leg movements and the locomotion control system of our model so that it produced gait transition and hysteresis, but because the stability structure changed through dynamic interactions among the body mechanical system, the nervous system, and the environment.

The CPGs in biological systems can produce oscillatory motor commands even without rhythmic input and proprioceptive feedback. However, adequate sensory regulation of motor commands is required to generate adaptive and effective locomotion. The locomotor rhythm and phase have been shown to be modulated by producing phase shift and rhythm resetting based on sensory afferents and perturbations (phase resetting) [32,39,46–48]. In addition, spinal cats achieve locomotion on treadmills and their gait varies with the belt speed [35,58], suggesting that tactile sensory information influences the locomotor rhythm and phase generated by the CPGs [59]. In this study, we used phase resetting for the sensory regulation model during locomotion. Without this sensory regulation, all the values of the relative phase Δ_{31} are neutral and the body mechanical system makes no contribution to the gait. Our sensory regulation model changed this stability structure so as to produce equilibrium points of Δ_{31}, where the three legs are synchronized at high speeds whereas the six legs are not synchronized at low speeds. A stability analysis using the return map clarified that the equilibrium points change through the saddle-node bifurcation, which induces hysteresis in the gait transition (Fig. 7).

Locomotion in biological systems involves a large number of degrees of freedom. Simple physical models constructed by extracting the fundamentals of their locomotion dynamics are useful to understand their locomotor mechanism [15,60–63]. In particular, stability and bifurcation structures obtained using simple models have provided meaningful biological insights [12,64]. We denoted the movement of one leg by the oscillator phase and reduced the degrees of freedom of the gait by employing biologically adequate constraints, which enabled us to clarify the stability and bifurcation structures of locomotion dynamics in our model. We intend to develop a more biomechanically and physiologically sophisticated model of insects to better understand the gait transition mechanisms in locomotion dynamics.

ACKNOWLEDGMENTS

This paper is supported in part by a Grant-in-Aid for Scientific Research (B) (Grant No. 23360111) and a Grant-in-Aid for Challenging Exploratory Research (Grant No. 23656185) from the Ministry of Education, Culture, Sports, Science, and Technology of Japan.

[1] R. Alexander, Physiol. Rev. **69**, 1199 (1989).
[2] F. Diedrich and W. Warren, Jr., J. Exp. Psychol. Hum. Percept. Perform. **21**, 183 (1995).
[3] D. Wilson, Annu. Rev. Entomol. **11**, 103 (1966).
[4] S. Aoi, D. Katayama, S. Fujiki, N. Tomita, T. Funato, T. Yamashita, K. Senda, and K. Tsuchiya, J. R. Soc. Interface **10**, 20120908 (2013).
[5] T. Griffin, R. Kram, S. Wickler, and D. Hoyt, J. Exp. Biol. **207**, 4215 (2004).
[6] A. Hreljac, R. Imamura, R. Escamilla, and W. Edwards, Gait Posture **25**, 419 (2007).
[7] C. Lamoth, A. Daffertshofer, R. Huys, and P. Beek, Hum. Mov. Sci. **28**, 371 (2009).
[8] A. Raynor, C. Yi, B. Abernethy, and Q. Jong, Hum. Mov. Sci. **21**, 785 (2002).
[9] V. Segers, P. Aerts, M. Lenoir, and D. Clercq, Gait Posture **24**, 247 (2006).
[10] N. Heglund and C. Taylor, J. Exp. Biol. **138**, 301 (1988).
[11] M. Turvey, K. Holt, M. LaFlandra, and S. Fonseca, J. Mot. Behav. **31**, 265 (1999).
[12] S. Aoi, T. Yamashita, and K. Tsuchiya, Phys. Rev. E **83**, 061909 (2011).
[13] H. Cruse, T. Kindermann, M. Schumm, J. Dean, and J. Schmitz, Neural Netw. **11**, 1435 (1998).
[14] Ö. Ekeberg, M. Blümel, and A. Büschges, Arthropod Struct. Dev. **33**, 287 (2004).
[15] P. Holmes, R. Full, D. Koditschek, and J. Guckenheimer, SIAM Rev. **48**, 207 (2006).
[16] R. Kukillaya, J. Proctor, and P. Holmes, Chaos **19**, 026107 (2009).
[17] K. Ohgane and K. I. Ueda, Phys. Rev. E **77**, 051915 (2008).
[18] K. Ohgane and K. I. Ueda, Phys. Rev. E **81**, 041909 (2010).
[19] K. Pearson, Ö. Ekeberg, and A. Büschges, Trends Neurosci. **29**, 625 (2006).
[20] J. Proctor, R. Kukillaya, and P. Holmes, Phil. Trans. R. Soc. A **368**, 5087 (2010).
[21] G. Taga, Y. Yamaguehi, and H. Shimizu, Biol. Cybern. **65**, 147 (1991).
[22] T. Tóth, S. Knops, and S. Daun-Gruhn, J. Neurophysiol. **107**, 3267 (2012).
[23] T. Wadden and Ö. Ekeberg, Biol. Cybern. **79**, 161 (1998).
[24] J. Bender, E. Simpson, B. Tietz, K. Daltorio, R. Quinn, and R. Ritzmann, J. Exp. Biol. **214**, 2057 (2011).
[25] F. Delcomyn, J. Exp. Biol. **54**, 443 (1971).
[26] D. Graham, Biol. Cybern. **26**, 187 (1977).
[27] D. Jindrich and R. Full, J. Exp. Biol. **202**, 1603 (1999).
[28] K. Pearson, Sci. Am. **235**, 72 (1976).
[29] J. Collins and I. Stewart, Biol. Cybern. **68**, 287 (1993).
[30] R. Ghigliazza and P. Holmes, SIAM J. Appl. Dyn. Syst. **3**, 671 (2004).
[31] S. Kimura, M. Yano, and H. Shimizu, Biol. Cybern. **69**, 183 (1993).
[32] U. Bässler and A. Büschges, Brain Res. Rev. **27**, 65 (1998).
[33] S. Grillner, Nat. Rev. Neurosci. **4**, 573 (2003).
[34] E. Marder and D. Bucher, Curr. Biol. **11**, R986 (2001).
[35] G. Orlovsky, T. Deliagina, and S. Grillner, *Neuronal Control of Locomotion: From Mollusc to Man* (Oxford University Press, Oxford, 1999).
[36] M. Shik and G. Orlovsky, Physiol. Rev. **56**, 465 (1976).
[37] R. Burke, A. Degtyarenko, and E. Simon, J. Neurophysiol. **86**, 447 (2001).
[38] M. Lafreniere-Roula and D. McCrea, J. Neurophysiol. **94**, 1120 (2005).
[39] I. Rybak, N. Shevtsova, M. Lafreniere-Roula, and D. McCrea, J. Physiol. **577**, 617 (2006).
[40] G. Bosco and R. Poppele, Physiol. Rev. **81**, 539 (2001).
[41] A. Casabona, M. Valle, G. Bosco, A. Garifoli, S. Lombardo, and V. Perciavalle, Brain Res. **972**, 127 (2003).
[42] R. Poppele, G. Bosco, and A. Rankin, J. Neurophysiol. **87**, 409 (2002).
[43] R. Poppele and G. Bosco, Trend. Neurosci. **26**, 269 (2003).
[44] F. Delcomyn and P. Usherwood, J. Exp. Biol. **59**, 629 (1973).
[45] M. Hoy and R. Zernicke, J. Biomech. **18**, 49 (1985).
[46] B. Conway, H. Hultborn, and O. Kiehn, Exp. Brain Res. **68**, 643 (1987).
[47] J. Duysens, Brain Res. **133**, 190 (1977).
[48] E. Schomburg, N. Petersen, I. Barajon, and H. Hultborn, Exp. Brain Res. **122**, 339 (1998).
[49] S. Aoi, N. Ogihara, T. Funato, Y. Sugimoto, and K. Tsuchiya, Biol. Cybern. **102**, 373 (2010).
[50] S. Aoi, T. Kondo, N. Hayashi, D. Yanagihara, S. Aoki, H. Yamaura, N. Ogihara, T. Funato, N. Tomita, K. Senda *et al.*, Biol. Cybern. **107**, 201 (2013).
[51] S. Yakovenko, V. Gritsenko, and A. Prochazka, Biol. Cybern. **90**, 146 (2004).
[52] T. Nomura, K. Kawa, Y. Suzuki, M. Nakanishi, and T. Yamasaki, Chaos **19**, 026103 (2009).
[53] S. Strogatz, *Nonlinear Dynamics and Chaos: With Applications to Physics, Biology, Chemistry, and Engineering* (Perseus Books, New York, 1994).
[54] C. Farley and C. Taylor, Science **253**, 306 (1991).
[55] S. Wickler, D. Hoyt, E. Cogger, and G. Myers, J. Exp. Biol. **206**, 1557 (2003).
[56] C. Spirito and D. Mushrush, J. Exp. Biol. **78**, 233 (1979).
[57] T. Tang and D. Macmillan, J. Exp. Biol. **125**, 107 (1986).
[58] H. Forssberg and S. Grillner, Brain Res. **50**, 184 (1973).
[59] J. Duysens, F. Clarac, and H. Cruse, Physiol. Rev. **80**, 83 (2000).
[60] H. Geyer, A. Seyfarth, and R. Blickhan, Proc. R. Soc. B **273**, 2861 (2006).
[61] A. Ijspeert, A. Crespi, D. Ryczko, and J. Cabelguen, Science **315**, 1416 (2007).
[62] J. Nishii, J. Theor. Biol. **238**, 636 (2006).
[63] M. Srinivasan and A. Ruina, Nature (London) **439**, 72 (2006).
[64] S. Aoi, Y. Egi, and K. Tsuchiya, Phys. Rev. E **87**, 012717 (2013).